An Advanced Displacement-Confinement Method for Design of Mechanized Shield Tunnels in Soft Ground

Eden Almog-Goldreich[a,b], Raul Fuentes[a]

[a] *Institute of Geomechanics and Underground Technology (GUT), RWTH Aachen University, Templergraben 55, Aachen, 52062, North Rhine-Westphalia, Germany*

[b] *Kiewit Engineering Group Canada ULC, 1425 North Service Rd E#1, Oakville, L6H 7E2, Ontario, Canada*

Abstract

This paper presents the Advanced Displacement-Confinement Method (ADCM), a semi-analytical framework for the design of mechanized shield tunnels in soft ground. The method bridges the gap between empirical design methods and full three-dimensional numerical analyses by providing a transparent, mechanistically informed workflow. ADCM integrates two new modules: the SHIELD model, which projects face and grout pressures onto the tunnel cross-section to define a circumferential distribution of applied loads and a confinement ratio index (λ_{TBM}); and the RINGS model, which describes ground convergence using a Mohr-Coulomb shear-hardening constitutive model which does not require an iterative solver. Together with conventional structural lining design models and empirical settlement transfer functions, these components allow direct evaluation of the relationships between TBM operation, ground response, lining loads, and surface settlements. The method is computationally efficient, requires only standard input parameters, and produces results consistent with case histories from soft ground shield tunnelling projects. Its scope is limited to short-term behaviour under closed-face conditions, but within this range ADCM offers a practical and reliable design tool that supports both preliminary assessments and parametric studies as well as accurate real-time back-analysis.

Keywords: Advanced Displacement-Confinement Method, Shield Tunnelling, Lining Design, Ground Movements.

1. Introduction

Soft ground tunnelling using shield Tunnel Boring Machines (TBMs) has become a cornerstone of modern infrastructure development, particularly in urban environments [1]. The success of these projects hinges on balancing two often competing objectives: minimizing ground movements with the associated risks to existing structures and optimizing the design of tunnel support and TBM operations to reduce costs and construction schedule.

Figure 1 presents a schematic of a typical soft ground TBM showing the key components and the various geometrical parameters adopted in this paper. Modern tunnel-induced movements arise mainly from two principal sources: ground loss ahead of the face, which includes consideration of the earth or slurry pressures, the overcut and shield taper gap where bentonite injections are often performed; and soil convergence due to the gap between the lining and the ground at the tail of the shield in which continuous backfill grouting is performed at a pressure which is proportional to the advance rate [2], [3]. Recent case histories such as [4] and [5] demonstrate that the lining deformations typically contribute to less than 10%–15% of the ground loss and that most of the short-term ground relaxation can be assumed to conclude at the first set of installed lining rings. Conversely, the ground loss has a significant impact on the lining design as it reflects the amount of stress relaxation and anisotropic ground response.

Well-established semi-empirical methods such as [6] or [7] and elastic analytical methods such as [8] and [9], can predict the total surface movements from an assumed ground loss with excellent accuracy, but fall short of a rigorous analysis of the overall and individual tunnelling processes and TBM operations, soil behaviour and the impact on the lining demands and deformations. They are therefore incomplete solutions with one particular purpose and cannot be considered adequate tools for tunnel design.

Classic Convergence-Confinement Method (CCM) isotropic solutions such as [10] and [11], address the relationship between radial deformations and ground loading based on an elastic-perfectly plastic constitutive model. Recent advancements by [12], [13] and

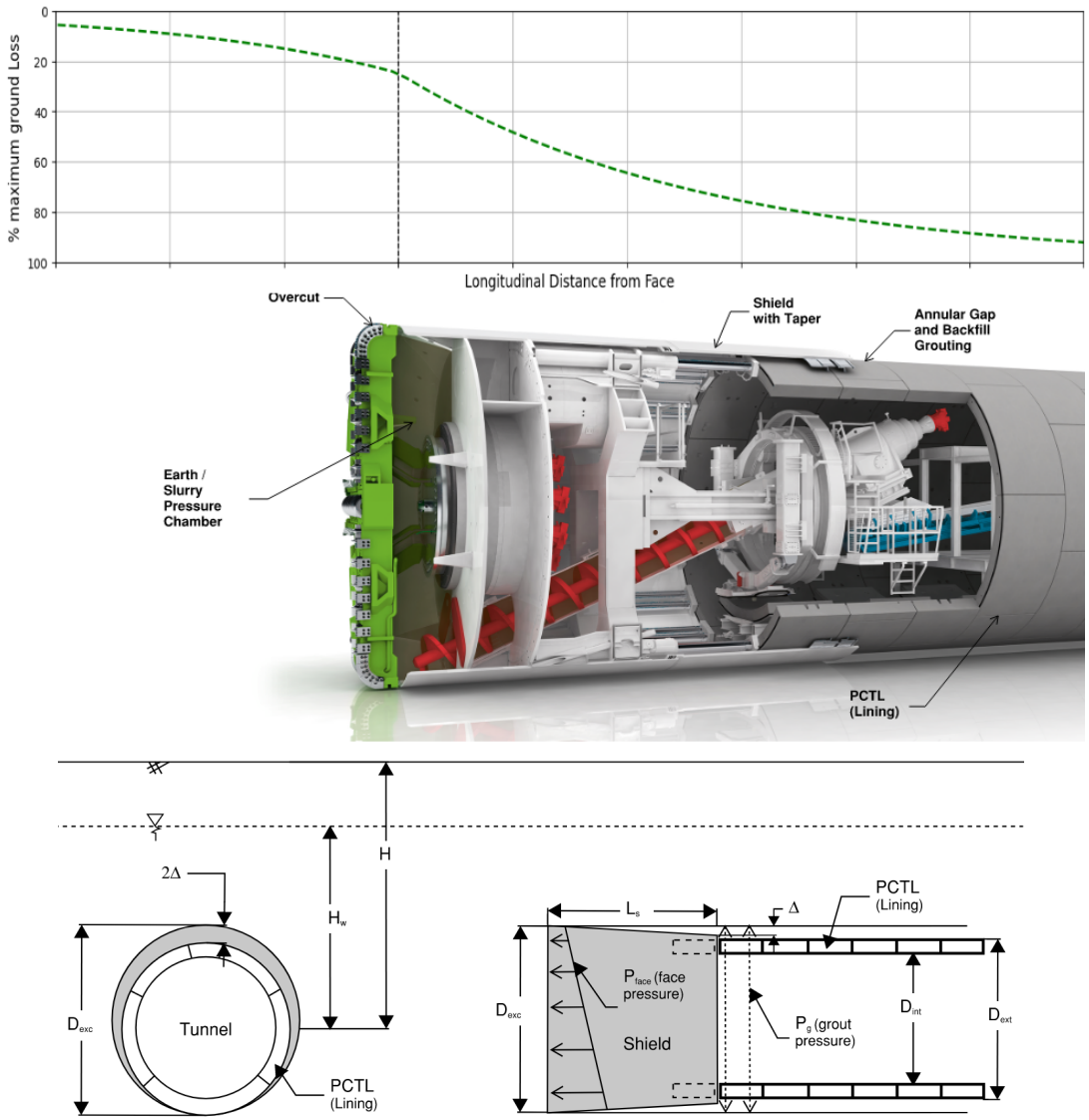

Figure 1: Schematic of (top) Closed face Earth Pressure Balance (EPB) machine and ground interaction components (machine image: www.herrenknecht.com), and (bottom) Tunnel geometry and TBM parameter definitions.

[14] extend these CCM models to non-linear soil behaviour albeit with some significant simplifications. Solutions by [15] and [16] extend the CCM to an anisotropic stress state in an elastic-perfectly plastic material. None of these solutions assume internal TBM pressure or shield interaction. They are thus useful approximations for estimating the ground convergence around relatively small diameter deep tunnels in hard ground excavated using open-face tunnelling and are not applicable to soft ground shallow closed-face urban tunnelling.

The analytical CCM solution by [17], builds on the work by [18] and modifies the CCM

solutions by [19] and [20] to account for an isotropic TBM pressure in elastic-perfectly plastic soil by introducing the TBM Confinement Ratio (λ_{TBM}) concept. The method is one of the few solutions used in practice that accommodates for the TBM face pressure and is thus of critical importance for the development of the method presented in this paper. However, due to the simple material model and isotropic insitu and TBM pressures, lack of consideration of grouting pressures or shield interaction, it shares many of the limitations of all CCM solutions and is thus only applicable to deep or smaller diameter TBMs of a specific type and geometry.

Many practitioners rely on full 3D numerical models like [21] or [22], the implementation of which to PCTL design is discussed in the ITA Working Group 2 report [23]. However these methods are computationally intensive, limiting parametric analyses and hindering real-time back-analysis. They also lack a consistent methodology across the industry, making results heavily dependent on software capabilities and the tunnel practitioner's modelling expertise. For example, the recent TULIP experiment and benchmark exercise [24] showed that five-fold differences can be encountered on results modelling TBM processes even when using the same input parameters. Also, use of numerical methods for design of geotechnical structures poses significant challenges with modern design codes, as discussed by [25], mainly due to the importance of capturing the initial state of stress in the ground with partial soil material factors and the inability to apply partial resistance factors. It remains to be seen if the new generation of the Eurocodes will address these limitations for soft ground shield tunnelling.

There is therefore a clear gap in the industry that requires a consistent design method for closed-face mechanized shield tunnels. This paper introduces a design methodology aimed at closing this gap.

2. The Advanced Displacement-Confinement Method

The Advanced Displacement-Confinement Method (ADCM) is a semi-analytical design approach specifically formulated for closed-face shield tunnelling in soft ground, linking the confinement provided by the TBM pressures, the ground-shield-lining interaction and surface movements. ADCM builds upon current methods, incorporating heuristic mathematical approximations that allow explicit considerations of TBM operations, ground response, and tunnel lining behaviour in line with current practise, but taking it one step forward beyond state-of-the-art. The method is conceived either as a stand-alone design framework or a complimentary tool for numerical modelling.

The novelty of ADCM lies in:

- A new systematic framework providing a consistent design chain: TBM operation $\longrightarrow$ ground loading $\longrightarrow$ lining $\longrightarrow$ settlements, that can also be reversed.
- Introducing the SHIELD circumferential confinement model to explicitly link TBM pressures (face + grouting) and providing an anisotropic ground relaxation to be used in a 2D plane strain analysis.
- Developing RINGS with a constitutive law, which bridges the gap between the overly simple Mohr-Coulomb and the more computationally demanding Hardening Soil model while incorporating the interaction with the TBM shield.

The main steps of the ADCM process are summarized in Table 1 and illustrated in Figure 2. The process is iterative targeting the optimal TBM operational parameters and allowable pressures (P_{TBM}^{SLS}) and most economical lining design. Critically, combined it covers all relevant processes present during TBM operation.

Component / Model	Description
Tunnel Geometry, Ground Conditions and Design Factors	This primary step in any tunnel design process is used to determine the governing ground conditions and geotechnical parameters and selection of the TBM type and its operational and geometrical parameters as well as the Precast Concrete Tunnel Lining (PCTL) configuration. The partial safety factors for loading and material parameters are set at this stage if the calculation is carried out as limit state design. Ultimate limit state face and grouting pressure range (P_{TBM}^{ULS}) are obtained based on well-established face stability and blowout calculations such as those in [26].
Soil-Hydraulic Initial Equilibrium and Load Distribution ("SHIELD")	A new two-dimensional closed-form confinement model simulating the stress state and anisotropic ground load controlled by TBM excavation and support pressure, prior to stress relaxation. The model's primary output is the TBM Confinement Ratio (λ_{TBM}), which is the amount of ground relaxation as a function of the anisotropic TBM confinement and ground stress state. The parameter is also used as an index for assessing optimal face pressures.
Radial Increments of Nonlinear Ground Stabilization ("RINGS")	A new CCM-based explicit algorithm that calculates the elasto-plastic radial and tangential strain field due to stress relaxation around the TBM via a new shear-hardening constitutive model accounting for the closure of the overcut and shield radial gap. The primary outputs of the model are the anisotropic relaxed effective ground radial stress acting on the tunnel lining and the soil stiffness.
PCTL Structural Model	The outputs from RINGS are utilized as an input into existing closed-form analytical solutions, bedded-spring, or finite element structural models to obtain the lining forces and deformations. While a closed form solution is adopted in this paper, the choice of which model to use is flexible and left open to the design engineer along with the level of sophistication and detail for simulating the PCTL behaviour.
Surface Deformation Model	The total volume loss combining the ground convergence from RINGS together with the lining deformations is used as an input into empirical solutions or numerical models which incorporate surface structures to obtain the settlement trough and maximum surface settlement (S_{max}). It is then possible to set monitoring trigger levels for the TBM drive with the assistance of the Displacement-Confinement Curve (DCC) and any impact assessment on surface structures.

Table 1: ADCM components and descriptions

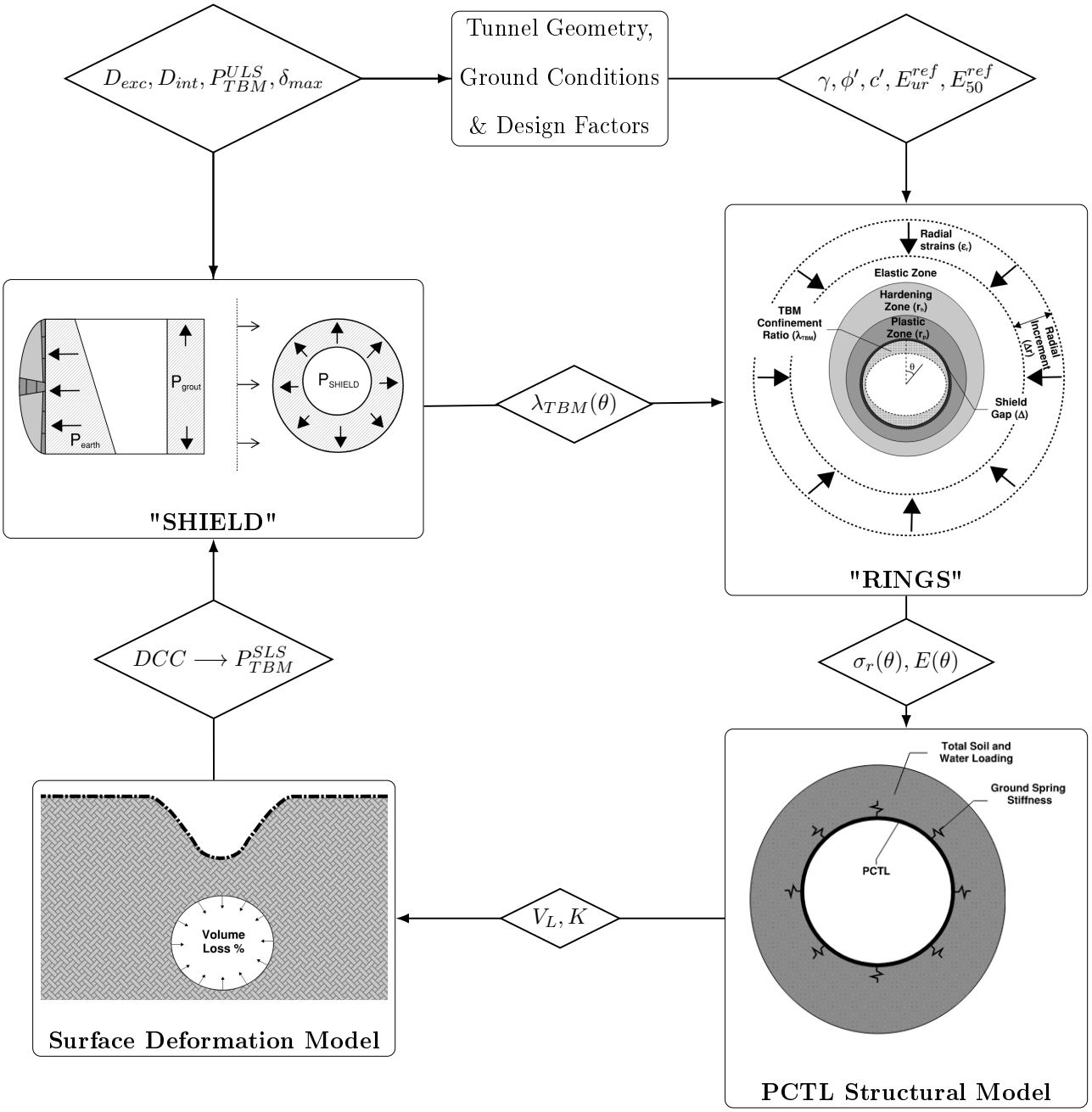

Figure 2: ADCM process flowchart and key outputs

2.1. SHIELD Model

The SHIELD model is introduced to approximate the circumferential distribution of TBM and grout pressures by projecting the three-dimensional face earth or slurry pressure and tailskin injection system onto the two-dimensional tunnel cross-section. The model combines face pressure, grout pressure distribution, and anisotropic soil in-situ stresses into

an explicit formulation of the TBM confinement ratio, a design index linking operational pressures with ground response.

2.1.1. TBM Pressure Calculation

The starting point is the face pressure. This is the pressure applied at the cutterhead and varies with angular position θ around the tunnel perimeter:

$$P_{face}(\theta) = P_{TBM} - 0.5 \cdot D_{exc} \cdot \gamma_{bt} \cdot \cos(\theta) \tag{1}$$

Where:P_{TBM} is the TBM face pressure at springline, θ is the angular position around the shield, D_{exc} is the shield diameter, and γ_{bt} is the unit weight of the bentonite or slurry.

The face pressure is then adjusted to account for the tailskin grout pressure. This is introduced as an amplification term as follows:

$$P_{SHIELD}(\theta) = P_{face}(\theta) + A \cdot f(\theta) \tag{2}$$

Where A is the grout pressure amplitude resulting from the mechanical work of the grout volume injected and $f(\theta)$ is a dimensionless shape function of the grout pressure distribution. This gives the first link between TBM operations (grout injection) and the anisotropic load distribution on the ground.

The average grout force per unit length of tunnel excavation is then defined. This force depends on the pressure difference between grout and face, the shield length, and the effective influence length of the grout as shown below:

$$F_g = \frac{\Delta P \cdot \pi \cdot D_{ext} \cdot L_g}{L_s} \tag{3}$$

Where we define ΔP as the difference between grout and face pressures, L_s as the length of the shield, and $L_g = L_s \cdot \frac{\Delta P}{P_{TBM}}$ as the influence length of the grout pressure.

ΔP is a function of the TBM advance rate as it controls the volume of grout that needs to be pumped at a minimum rate to fill the radial void around the PCTL. The relationship between the grout pressure and the TBM advance rate is captured by the grouting model by [3] who proposed an analytical relationship for obtaining P_g. Equation [4] solves it by setting $x = P_g - P_w$, where P_w is the ambient groundwater pressure at the injection point:

$$3r_i^4 x^4 - \left(\frac{48\mu v L r_0 h_g \xi}{n} + 8\tau_0 r_i^3 L\right) x^3 + 16\tau_0^4 L^4 = 0 \tag{4}$$

Where μ represents the dynamic viscosity of the grout and τ_0 denotes the yield stress of the grout. The TBM shield advance rate is given by v, and L corresponds to the length of the grout injection pipe. The excavated radius is denoted as $r_0 = \frac{D_{exc}}{2}$, and h_g represents the vertical height of the grout pipe system. The grout overfilling ratio, ξ, is a dimensionless parameter typically ranging from 1 to 2. The number of active grout injection lines is indicated by n, and r_i refers to the inner radius of each grout injection pipe. This relation describes the pressure required to mobilize grout flow through the injection system at the TBM advance rate.

The differential pressure between the grouting pressure and the average TBM face pressure was already defined as:

$$\Delta P = P_g - P_{TBM} \tag{5}$$

Note that the SHIELD model assumes a positive pressure boost and therefore if $P_g \leq P_{TBM}$ then $\Delta P = 0$ is enforced. This however is a rare case mostly observed in tunnelling in stiff clays with no active pore pressure as reported by [4]. It is also noted that grout consolidation can be accounted for by modifying the mechanical parameters of equation [4]. A rigorous numerical model for calculation of grout consolidation is given by [27].

To distribute the grout effect circumferentially, an empirical shape function is introduced:

$$f(\theta) = \left[\frac{1 - \cos(\theta)}{1 - \cos(\pi)}\right]^{m_g} = \left[\frac{1 - \cos(\theta)}{2}\right]^{m_g} \tag{6}$$

Where m_g is a newly proposed empirical positive exponent that controls the level of anisotropy in the TBM pressure and is governed by the tailskin grouting injections. In accordance with the work by [27], $m_g > 0$ corresponds to a model where the grout pressure is injected below springline. In practice however, it has been observed that setting $m_g = 1$ is most suitable for slurry TBMs while $m_g = 0$ is more suited for earth pressure balance (EPB) machines. This is because for slurry TBMs, the pressure at the face also acts around the shield gap limiting the influence the grout pressure, particularly at the crown.

The grout pressure amplitude, A, is then obtained by ensuring that the average pressure boost equals the distributed grout force over the mean of the shape function multiplied by the shield length:

$$A = \frac{F_g}{\overline{f}(\theta) \cdot L_s} \tag{7}$$

Where $\overline{f}(\theta) = \frac{1}{\pi} \int_0^{\pi} \left(\frac{1-\cos(\theta)}{2} \right)^{m_g} d\theta$, is a dimensionless constant for a given m_g value.

The final SHIELD pressure distribution around the cross-section is:

$$P_{SHIELD}(\theta) = (P_{TBM} - \frac{D_{exc} \cdot \gamma_{bt} \cdot \cos\theta}{2}) + \frac{\Delta P^2 \cdot \pi \cdot D_{exc}}{P_{TBM} \cdot L_s \cdot \overline{f}(\theta)} \cdot \left[\frac{1 - \cos\theta}{2} \right]^{m_g} \tag{8}$$

This combines the face pressure distribution (first term) with the grout amplification (second term). Note that when $m_g = 0$ (e.g., some EPB machines), the second term of equation [8] simplifies to $\frac{\Delta P^2 \cdot \pi \cdot D_{exc}}{P_{TBM} \cdot L_s}$ giving a constant pressure boost around the shield.

Equation [8] may yield unrealistically high pressure boosts when the grout pressure strongly exceeds the face pressure, especially at low face pressure levels. In such cases the calculated circumferential pressure can become greater than the actual grout pressure available at the extrados, which is physically impossible. To prevent this, a cap condition ensures that the maximum pressure applied around the circumference is always bounded by the grout pressure at the tunnel extrados:

$$P_{SHIELD}(\theta) \leq P_{face}(\theta) + \Delta P = P_g(\theta) \tag{9}$$

Figure 3 illustrate this effect: without the cap, SHIELD predicts pressures that can exceed grout injection pressure; with the cap, the curves remain consistent with measured ranges. It also shows how advance rate influences grout pressure and, consequently, the SHIELD distribution.

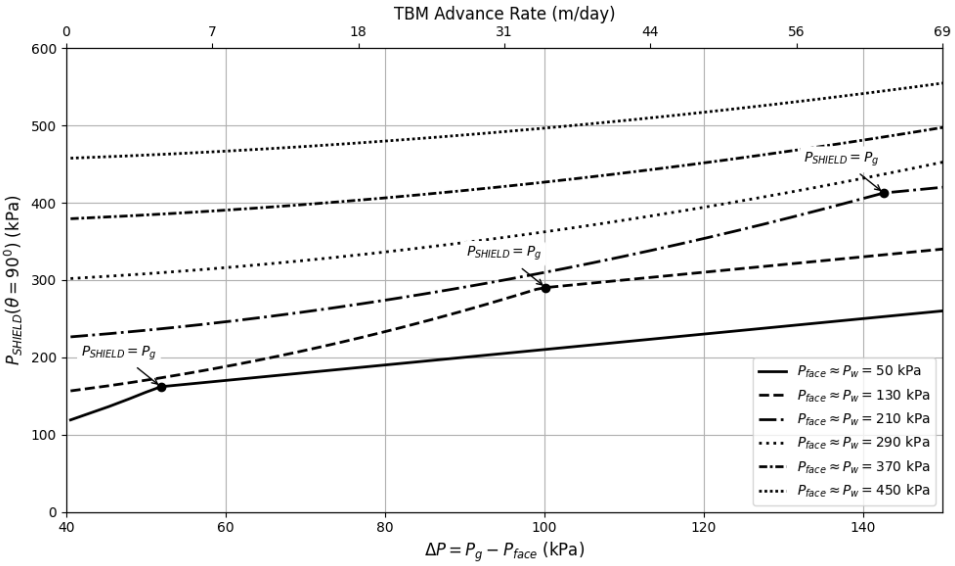

Figure 3: SHIELD pressure as function of ΔP and TBM Advance Rate ($m_g = 0$). It is assumed that the face pressure is equal to water pressure and a mid-size 8m dia. TBM with a 12m long shield and backfill grout material and system parameters taken from [3].

As shown, the SHIELD model allows to calculate a 2D circumferential pressure as a function of the face and grout pressures, and rate of the TBM advance - therefore linking the main TBM operational parameters to a single analytical confinement model. This greatly simplifies the calculation process and is critical in facilitating a plane strain, rather than a full 3D analysis.

2.1.2. TBM Confinement Ratio

In addition to the TBM internal pressure, a model for the external initial ground load distribution and the maximum ground relaxation is required. This is achieved by developing the TBM confinement ratio (λ_{TBM}) introduced by [17] for isotropic states, to account for an anisotropic stress state.

The soil's anisotropic ground effective confining stress at each angle θ is given by the

Kirsch solution:

$$P'_{soil}(\theta) = \frac{1}{2}\left[(\overline{\sigma}'_v + \overline{\sigma}'_h) - (\overline{\sigma}'_h - \overline{\sigma}'_v) \cdot cos(2\theta)\right] \tag{10}$$

where $\overline{\sigma}'_v = \gamma_{soil} \cdot z - \overline{u}$ is the average vertical soil effective stress, $\overline{\sigma}'_h = K_{TBM} \cdot \overline{\sigma}'_v$ is the average horizontal soil effective stress, and $\overline{u}$ is the average hydrostatic water pressure. The mobilized horizontal stress ratio $K_{TBM}(\theta)$, as per DAUB [26] recommendations, lies between the in-situ stress ratio K_0 and the Rankine active stress ratio $K_a = \frac{1-sin(\phi)}{1+sin(\phi)}$. For most practical cases, it can be assumed that K_{TBM} lies between 0.3 and 0.5.

The effective TBM SHIELD pressure around the tunnel extrados at each angle θ is:

$$P'_{SHIELD}(\theta) = P_{SHIELD}(\theta) - (\overline{u} - \gamma_w \cdot r_0 \cdot cos\theta) \tag{11}$$

The anisotropic TBM confinement ratio is then defined as follows:

$$\lambda_{TBM}(\theta) = 1 - \left(\frac{P'_{SHIELD}(\theta)}{P'_{soil}(\theta)}\right), \quad 0 \leq \lambda_{TBM}(\theta) \leq 1 \tag{12}$$

This more general form reduces to the isotropic case when $K_{TBM} = 1$ and $P_{SHIELD} = P_{TBM}$ giving a constant value: $\lambda_{TBM} = 1 - \frac{P'_{TBM}}{P'_{soil}}$. This particular case is applicable for situations of high face pressures where the influence of the grouting pressure is reduced, as in the case of deep tunnels.

2.1.3. Index for Optimal Face Pressures

The circumferential pressure provides a tractable way of incorporating the combined anisotropy of soil stress state and grout/face pressures into a single parameter. The λ_{TBM} can thus be utilized as index quantifies the adequacy of the chosen TBM earth and grout pressures when considering the condition at the tunnel crown:

- $\lambda_{TBM}(\theta = 0°) \rightarrow 1$: Under-Pressurized State: TBM pressures are too low, soil is largely relaxed, risking settlements or face instability.

- $\lambda_{TBM}(\theta = 0°) \rightarrow 0$: Over-Pressurized State: TBM pressures are too high, soil remains confined, but risks include blowout, excessive shield thrust and tool wear.
- $0.2 \leq \lambda_{TBM}(\theta = 0°) \leq 0.8$: Optimal Pressure State: This intermediate range generally provides a safe balance and corresponds with DAUB stability envelopes [26].

We stress here that λ_{TBM} is not intended as a mechanical description of soil response, but as a relaxation constant and design index for pressure adequacy, analogous to the long-used ground response curve in rock tunnelling. Its merit lies in its simplicity and in being calibrated against face stability checks along the tunnel alignment. This offers practitioners a quick stability and settlement risk assessment, which 3D FEM cannot provide at the same efficiency.

2.1.4. Model Behaviour

Figure 4 and Figure 5 show circumferential SHIELD pressures and λ_{TBM}. An example case of a 30m deep, 8m dia TBM with a 12m long shield, and grouting pressure 1 bar above face pressure is analyzed. Cases investigated assume $K_{TBM} = 0.5$ and $K_{TBM} = 1$ and $m_g = 0$ and 1 with a cap pressure $P_{max} = 5$ bar.

For $m_g = 0$, the SHIELD pressure is relatively uniform around the tunnel perimeter, resulting in a more balanced λ_{TBM} distribution and moderate ground relaxation compared with $m_g = 1$. The mobilized horizontal stress ratio (K_{TBM}) plays a critical role for the distribution of λ_{TBM}. Lower K_{TBM} values reduce horizontal stresses, leading to lower λ_{TBM} values and lower ground relaxation. Conversely, higher K_{TBM} values increase horizontal confinement, increasing λ_{TBM} and ground relaxation. As shown in the plots, higher K_{TBM} values result in more relaxation below the crown, eventually leading to overall higher volume losses and wider settlement troughs at the surface. Additionally, lower K_{TBM} values indicate conditions closer to high TBM pressures around the axis level, while at lower TBM pressures, it approaches $\lambda_{TBM} = 0$ conditions.

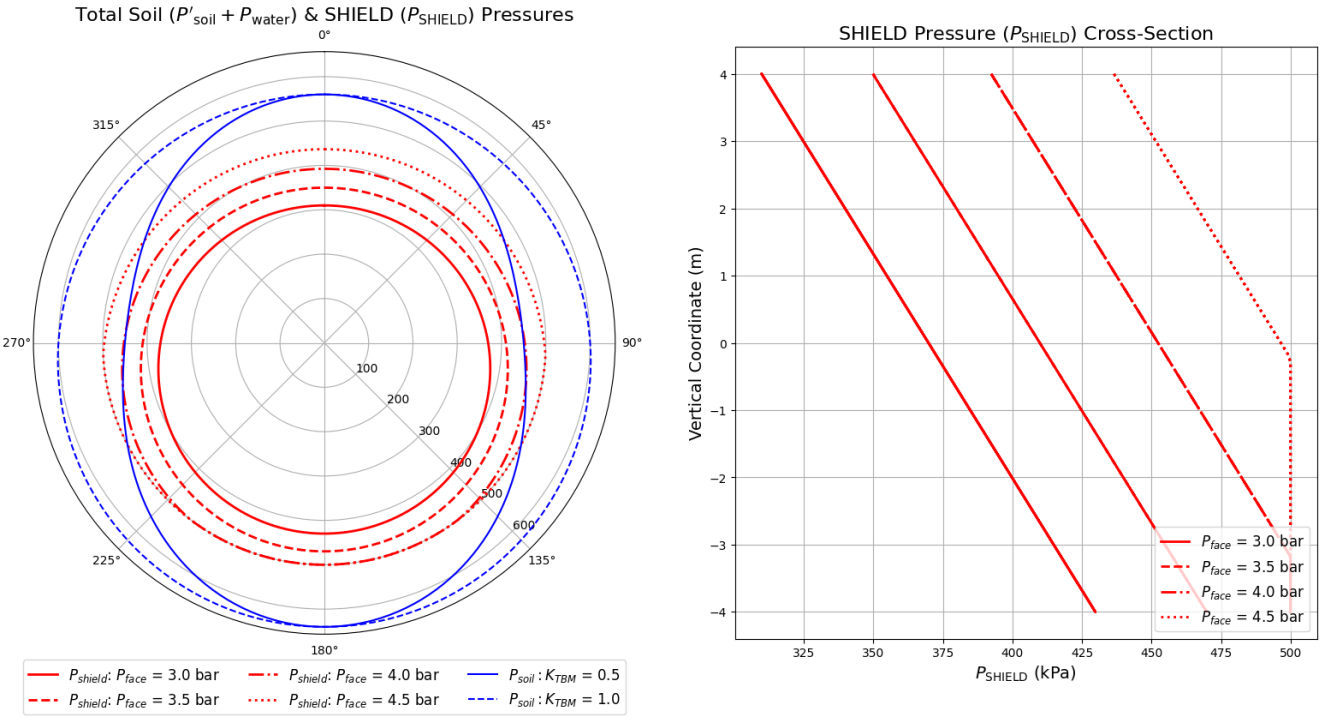

(a) SHIELD pressure distribution

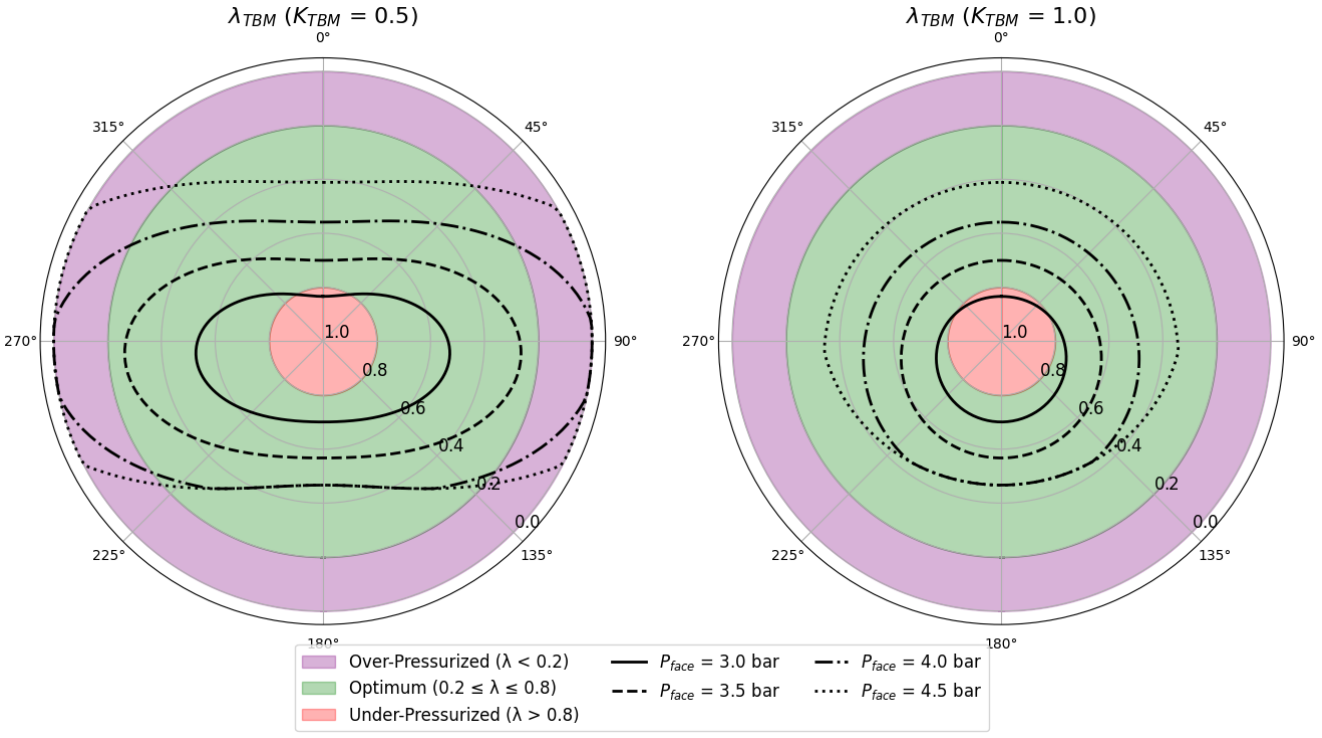

(b) λ_{TBM} distribution

Figure 4: SHIELD model circumferential plots for $m_g = 0$

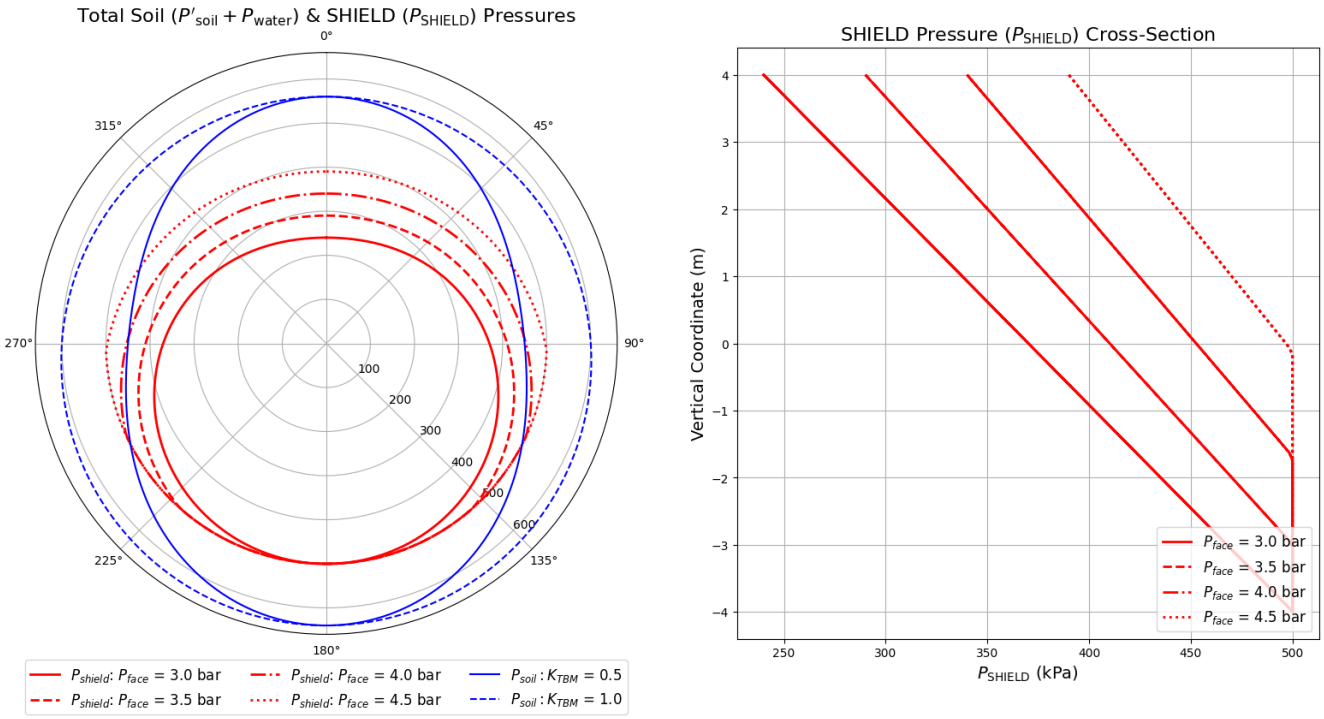

(a) SHIELD pressure distribution

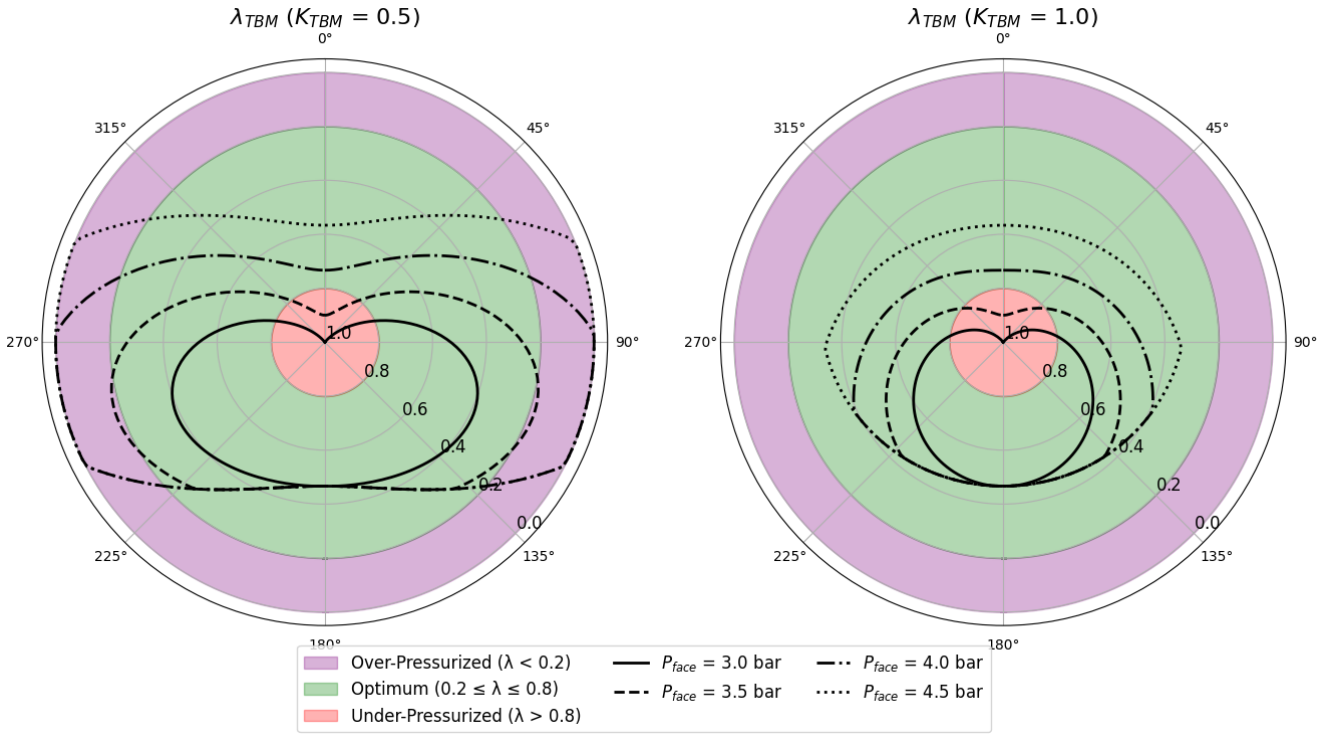

(b) λ_{TBM} distribution

Figure 5: SHIELD model circumferential plots for $m_g = 1$

2.2. RINGS Algorithm

RINGS is a semi-analytical explicit algorithm designed to calculate the radial and tangential stress and strain fields around a tunnel. It simulates the evolution of the stress state from initial conditions to a stabilized ground-support condition through incremental calculations of strains, progressing from the far field to the tunnel extrados. The algorithm accounts for the interaction of the soil with the shield by scaling the Longitudinal Displacement Profile (LDP) based on the the TBM shield gap and overcut.

Soil behavior in RINGS is modeled using a new semi-analytical effective stress constitutive law, referred to as the Mohr-Coulomb with Shear Hardening (MCSH) model. The MCSH is designed to capture the progressive shear mobilization that governs ground relaxation around advancing shield. Plastic strains and the hardening function are calculated incrementally, founded on the method implemented in the Simplified Hardening Soil (SHS) model by [13]. However unlike the SHS model, the MCSH formulation enables the calculation of both finite shear-hardening and plastic radii. This is achieved using the perfectly plastic solution for radial stress and a Critical Relaxation Ratio, as proposed by [15], to initiate plasticity. This eliminates the need for iterative numerical solvers which are highly non-linear and unsuitable for implementing partial load and resistance factors [25], as well as exhibiting numerical convergence issues at high levels of strength mobilization [28]. In addition, the exact solution for the perfectly-plastic radius, allows to utilize the LDP solutions by [19] to calculate the displacement ahead of the face and impose the limit for the shield gap as will be shown later.

2.2.1. Approximations and Limitations of the MCSH

Advanced numerical constitutive models such as HS and HS-small are widely used in finite element back-analyses of tunnel induced ground movements (e.g. [29], [30], [31] and [32]). It is often argued that the small-strain stiffness component is important for matching precise settlement trough shapes observed in monitoring data when using a numerical model.

The MCSH model however, deliberately excludes small-strain stiffness. Instead, it focuses on stress-dependent stiffness and non-linear shear hardening, which are the dominant mechanisms for short-term soil response as implemented in the isotropic SHS model by [13] and simulates stress anisotropy by utilizing the TBM Confinement Ratio (λ_{TBM}) as an anisotropic stress relaxation constant.

The following points provide more insight into the rationale behind omission of the small-strain stiffness in the MCSH model:

- The key premise of the ADCM, is that it is possible to achieve excellent agreement for ground movements for a wide range of soils, when the anisotropic hydraulic-soil interaction around the advancing TBM shield is properly accounted for. This is altogether not a new observation as discussed in the formulation of the well established semi-empirical and analytical models such as [6] and [9].

- As already introduced in Section 1 and explained further in Section 4, the RINGS algorithm primary function is to provide the relaxed anisotropic ground loading on the PCTL and the volume loss. The calculated volume loss can be inserted into empirical solutions which can produce a very good match to the settlement trough, rather than obtain it directly from the displacement field, which may be affected by the small-strain stiffness aspects, especially in over-consolidated clays [33].

- Advanced numerical models such as the HS-small or BRICK [33] require specialized geotechnical investigations and extensive parameterization (e.g., strain-dependent stiffness curves, initial shear modulus and reference strain), which are not always possible and often have schedule impacts on projects delayed due to superfluous in-situ or laboratory testing. They also impose computational costs and are generally difficult to validate. In fact, we find it has become increasingly challenging to justify the use of small-strain stiffness models during the design and construction phases of most tunnelling projects.

In addition to the omission of small-strain stiffness, the MCSH model does not account for

isotropic hardening due to increases in mean effective stress or the effects of excess pore pressures. RINGS and the MCSH model are positioned as short-term, operational design tools. Shield tunneling is governed by transient stress redistribution, where excess pore pressures are actively countered by earth or slurry pressures exceeding hydrostatics [26]. Observations from multiple case studies (see Section 5) confirm that post-TBM consolidation contributes minimally to greenfield settlements. Most movements are controlled by TBM support pressure and the shield gap. This limitation is therefore not critical for closed-face TBMs and MCSH has proven sufficiently robust to capture stresses and strains in most soft ground conditions and outperforms the standard Mohr-Coulomb (MC) model due to its stress-dependent stiffness and non-linear shear hardening law.

For long-term settlement and groundwater-related effects, we do recommend complementary numerical analyses. These often complex analyses can be simplified by using the outputs of the SHIELD model and RINGS algorithm as inputs into a plane-strain fully coupled model, which is another contribution of this work.

2.2.2. Elastic Perfectly-Plastic Stress Field

The elastic and perfectly plastic radial and tangential stresses are derived via an approximation of the closed-form anisotropic solution by [15]. The anisotropic elastic stresses are written using the isotropic form of the solution (i.e. $K_0 = 1$) but with an anisotropic deconfinement ratio $\lambda = \lambda_{TBM}(\theta)$ calculated in SHIELD, which incorporates K_{TBM}:

$$\sigma_r^{el}(\theta) = \sigma'_v \cdot [1 - \lambda_{TBM}(\theta) \cdot (\frac{r_0}{r})^2] \tag{13}$$

$$\sigma_t^{el}(\theta) = \sigma'_v \cdot [1 + \lambda_{TBM}(\theta) \cdot (\frac{r_0}{r})^2] \tag{14}$$

Where σ'_v is the vertical soil effective stress at the tunnel springline, r_0 is the the largest excavated tunnel radius (i.e. cutterhead) and r is the radial distance away from the tunnel centre.

The solution for the perfectly plastic stresses begins by considering the equilibrium dif-

ferential equation for an axisymmetric plain-strain problem [13]:

$$\frac{d\sigma_r}{dr} = \frac{\sigma_\theta - \sigma_r}{r} \tag{15}$$

The MC strength criterion is expressed as follows:

$$\sigma_\theta = \sigma_r + K'(C + \sigma_r) \tag{16}$$

Where $K' = \frac{2\sin\phi}{1-\sin\phi}$, $C = c \cdot \cot\phi$, c: apparent cohesion, and ϕ: friction angle.

Substituting equation (15) into equation (16) and solving the integral for the elastic perfectly-plastic boundary at the plastic radius r_p we obtain the radial stresses on each side of the boundary:

$$\text{Plastic Side:} \quad \sigma_r^- = \left(C + \sigma_r^+\right) \cdot \left(\frac{r}{r_p}\right)^{K'} - C \tag{17}$$

$$\text{Elastic Side:} \quad \sigma_r^+ = \sigma_v' \left(1 - \lambda_{TBM}^e \cdot \left[\frac{r_p}{r}\right]^2\right) \tag{18}$$

Where λ_{TBM}^e is the Critical Deconfinement Ratio at which the level of radial stress deconfinement is high enough to initiate plasticity. This plastic constant is derived by inserting equation (17) and equation (18) into the equation (16) and setting $r = r_0$ at the initiation of plasticity around the tunnel extrados:

$$\lambda_{TBM}^e = \frac{\frac{K'C}{\sigma_v'} + (1 + K') - 2}{2[1 - (1 + K')]} \tag{19}$$

It is then now possible to obtain an expression for the plastic radius r_p by setting $r = r_0$ and the radial stress given by equation (17) equal to the radial stress given by equation (18) at the interface between the elastic and plastic regions and rearranging to obtain:

$$r_p(\theta) = r_0 \cdot \left(\frac{2 \cdot \sigma_v' \cdot (1 - \lambda_{TBM}^e) + C}{2 \cdot \sigma_v' \cdot (1 - \lambda_{TBM}(\theta)) + C}\right)^{\frac{1}{K'}} \tag{20}$$

As such, deconfinement increases until the term on the right-hand side becomes larger than 1, at which point plasticity initiates, and the plastic zone then expands beyond the excavated extrados with further deconfinement.

And so the full set of equations for the perfectly-plastic stresses outside and inside the plastic zone can be obtained as given in Table 2.

Plastic Stress	$r > r_p$	$r \leq r_p$
Radial	$\sigma_r^p(\theta) = \sigma_v' \left(1 - \lambda_{TBM}^e \cdot \left[\frac{r_p(\theta)}{r}\right]^2\right)$ (21)	$\sigma_r^p(\theta) = \left[(1-\lambda_{TBM}^e)\cdot\sigma_v' + C\right] \cdot \left(\frac{r}{r_p(\theta)}\right)^{K'} - C$ (22)
Tangential	$\sigma_\theta^p(\theta) = \sigma_v' \left(1 + \lambda_{TBM}^e \cdot \left[\frac{r_p(\theta)}{r}\right]^2\right)$ (23)	$\sigma_\theta^p(\theta) = \left[(1-\lambda_{TBM}^e)\cdot\sigma_v' + C\right] \cdot (1+K') \left(\frac{r}{r_p(\theta)}\right)^{K'} - C$ (24)

Table 2: Equations for Radial and Tangential Stresses in Elastic and Plastic Zones

2.2.3. Hardening Law

We introduce a semi-analytical algorithm in which the MC model is modified to incorporate the expanding shear yield surface from the HS model. Plastic strains and hardening function are calculated in increments again inspired by the algorithm deployed for the Simplified Hardening Soil (SHS) model by [13]. The fundamental HS model formulations are taken from [34] and [35] and are summarized in Table 3.

The normalized hardening function in eq.(30) serves as the hardening law while automatically enforcing a shear failure at the MC failure surface:

$$q_{yield} = \; q_a \; \cdot \; r_q \qquad \{q_{yield} \leq \; q_{elastic} \; , \quad r_q \leq R_f \; \} \tag{31}$$

The post-yield tangential stress is then:

$$\sigma_\theta^y = q_{yield} + \; \sigma_r \qquad \left\{ \begin{array}{l} \lambda_{TBM}\,(\theta) < \lambda_{TBM}^e : \; \sigma_r = \sigma_r^{el} \\ \lambda_{TBM}\,(\theta) \geq \lambda_{TBM}^e : \; \sigma_r = \sigma_r^p \end{array} \right\} \tag{32}$$

Description	Equation
Asymptotic Shear Stress	$q_a = \frac{q_f}{R_f}$ (25)
MC Shear Strength Criterion	$q_f = K'(C + \sigma_r)$ (26)
Stress Dependent Primary Loading Modulus	$E_{50} = E_{50}^{ref} \left(\frac{c \cot \phi + \sigma_r}{c \cot \phi + p_{ref}} \right)^m$ (27)
Stress Dependent Unloading-Reloading Stiffness	$E_{ur} = E_{ur}^{ref} \left(\frac{c \cot \phi + \sigma_r}{c \cot \phi + p_{ref}} \right)^m$ (28)
Shear Hardening Yield Function	$f_s = \frac{q_a}{2E_{50}} \frac{q}{q_a - q} - \frac{q}{E_{ur}} - \gamma_p = 0$ (29)
Normalized Hardening Function	$r_q = \frac{1}{2} \sqrt{\left(r_u - 1 + \frac{4\gamma_p E_{ur}}{q_a} \right)^2 + \left(\frac{4\gamma_p E_{ur}}{q_a} \right)} - \frac{1}{2} \left(r_u - 1 + \frac{4\gamma_p E_{ur}}{q_a} \right)$ (30)

Table 3: Fundamental relationships for the HS model shear hardening law, where: p_{ref} is the reference pressure often set to 1 atm, γ_p is the plastic hardening parameter, $r_u = E_{ur}/2E_{50}$ and R_f is the failure ratio usually equal to 0.9.

2.2.4. Flow Rule

The MCSH model employs the HS model's non-associative flow rule to obtain the strain field in an incremental fashion by accumulating plastic strains from the far field to the tunnel extrados.

The stress increment for each radial increment r_i from the far field radius r_∞ is given as: $\Delta\sigma_r = \sigma_r(r_i, \theta) - \sigma_r(r_{i-1}, \theta)$, $\Delta\sigma_\theta = \sigma_\theta(r_i, \theta) - \sigma_\theta(r_{i-1}, \theta)$; where $\sigma_r(r_i, \theta)$ and $\sigma_\theta(r_i, \theta)$ or each increment depend on whether r_i is inside the hardening or plastic zones.

The elastic strain increments are defined using the Hook constitutive law:

$$\Delta\varepsilon_r^{el} = \left(\frac{1}{2G} \right) \cdot \left[(1 - \nu) \Delta\sigma_r - \nu \Delta\sigma_\theta \right] \tag{33}$$

$$\Delta\varepsilon_{\theta}^{el} = \left(\frac{1}{2G}\right) \cdot \left[(1 - \nu)\,\Delta\sigma_{\theta} - \nu\Delta\sigma_{r}\right] \tag{34}$$

$$\Delta\gamma^{el} = \left|\Delta\varepsilon_{\theta}^{el} - \Delta\varepsilon_{r}^{el}\right| \tag{35}$$

Where shear modulus $G = \frac{E_{ur}}{2(1+\nu)}$.

The plastic strain increment is then calculated using a non-associative flow rule and the strain compatibility equation:

$$\Delta\varepsilon_{\theta}^{pl} = -\left(\frac{\Delta \mathrm{r}}{r}\right) \cdot \left(\gamma_{p} + \gamma^{el}\right) - \Delta\varepsilon_{\theta}^{el} \tag{36}$$

$$\Delta\varepsilon_{r}^{pl} = -K_{\psi} \cdot \Delta\varepsilon_{\theta}^{pl} \tag{37}$$

$$\Delta\gamma^{pl} = \left|\Delta\varepsilon_{\theta}^{pl} - \Delta\varepsilon_{r}^{pl}\right| \tag{38}$$

Where $K_{\psi} = \frac{1+sin(\psi_m)}{1-sin(\psi_m)}$ is the HS model mobilized dilatancy coefficient and ψ_m is the mobilized dilation angle, obtained via the algorithm presented in [34] which is not reproduced here.

For a circular tunnel, the radial displacement is then simply:

$$u_{r} = r \cdot \varepsilon_{\theta} \tag{39}$$

The calculation of ε_{θ} is thus carried out for each value of $\lambda_{TBM}(\theta)$ at increments of θ giving full the displacement field around the tunnel.

It is noted that the choice of the radial increments Δr or stepping of $\lambda_{TBM}(\theta)$ generally have no effect on the solution, except for very large Δr which reduce the accuracy of identifying the hardening radius. Choosing $r_{\infty} \geq 20 \cdot r_0$ and $\Delta \mathrm{r} \leq 0.25m$ has proven to provide sufficient accuracy for most practical applications. In addition, it is necessary to set the initial values or $\sigma_r[0]$ and $\sigma_\theta[0]$ equal to σ_v' and the rest of the parameters to zero in order to correctly simulate the accumulation of plastic strains. Finally, for clearly visualizing the shear hardening radius, a plastic tangential strain criteria of $\epsilon_t^p > 0.01\%$ is

applied although this has no effect on the calculations.

2.3. Comparison to the MC and HS model

The MCSH is compared to the standard MC and HS constitutive models implemented in the Bentley Plaxis2D commercial software, presented in Figure 6. The Plaxis2D and MCSH models were run with isotropic field stress, no internal pressure and soil parameters presented in Table 4. As the MC model uses a constant stiffness, the numerical models were run with $E_{MC} = E_{ur}$ and $E_{MC} = \frac{E_{ur}}{3}$ with $m = 0$. The HS and MCSH models were run with the common r_u value of 1.5.

The MCSH model essentially forms a hybrid between the HS and MC models. The elastic and polar stresses and radial displacements follow the MC model until the yield surface is reached. This transition is characterized by a reduction in peak deviatoric stresses and an increase in radial displacement due to the generation of plastic shear strains prior to reaching a perfectly plastic stress state, at which point all models follow the MC failure surface.

The sensitivity of the HS model to initial conditions is clearly illustrated. For an OCR of 1 (normally consolidated), plasticity is activated from the beginning (i.e. infinite yield radius) with lower polar stresses and a gradual transition to full plasticity. For an OCR of 2 (over-consolidated), yielding occurs after some initial elastic deformation, leading to a finite shear hardening radius and a clearer transition to fully plastic behaviour. This is because the HS model includes a complex interaction of two yield surfaces and a failure surface. It is noted that this interaction relies on the algorithm in the numerical software in which the plastic hardening parameter and the isotropic yield cap are initialized, which can have a significant impact on the results.

The MCSH does not incorporate isotropic hardening and is therefore similar to the MC in that it is not sensitive to the OCR or initial conditions. However as shown, it produces a similar response compared to the HS model, with total deformations mid-way between

the HS model's OCR range, which is an acceptable approximation.

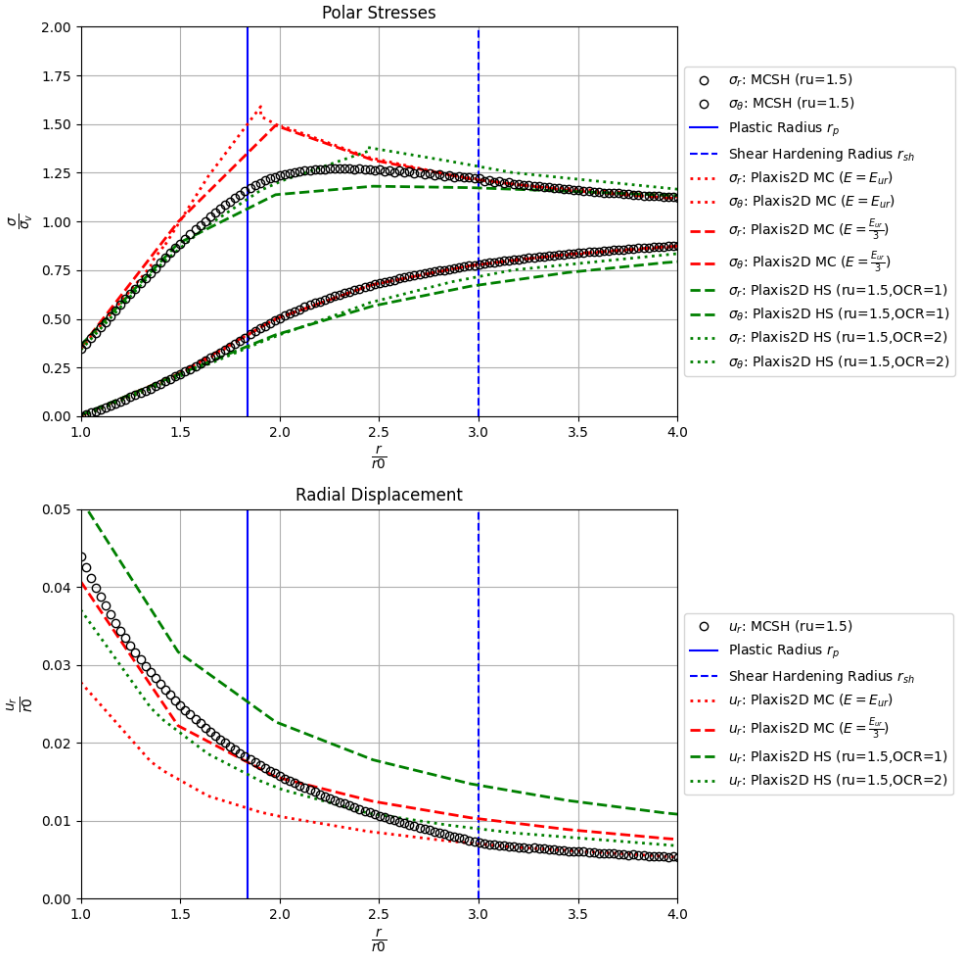

Figure 6: Comparison of MCSH to MC and HS models showing the polar stresses and displacement fields together with plastic and shear hardening radii as obtained from the MCSH model

Parameter	**Value**
Tunnel Radius (r_0)	4 m
Field Stress	100 kPa
Peak Friction Angle (φ)	30°
Peak Dilation Angle (ψ)	0°
Apparent Cohesion (c')	10 kPa
Reference Unload/Reload Modulus (E_{ur})	45 MPa
Stiffness Stress Dependency Factor (m)	0
Reference Pressure (p_{ref})	100 kPa
In-situ Stress Ratio (K_0)	1

Table 4: Input parameters for MCSH, HS and MC model comparison

2.4. Shield Interaction

The interaction with the shield controls the amount of deformation both ahead and behind the shield, thus limiting the ground loss and the deconfinement, and increasing the radial ground stresses. The RINGS model accounts for the shield interaction by scaling the

Longitudinal Displacement Profile (LDP) calculated without the shield, to the shield radial gap as illustrated in Figure 7. The LDP without the shield interaction is given by

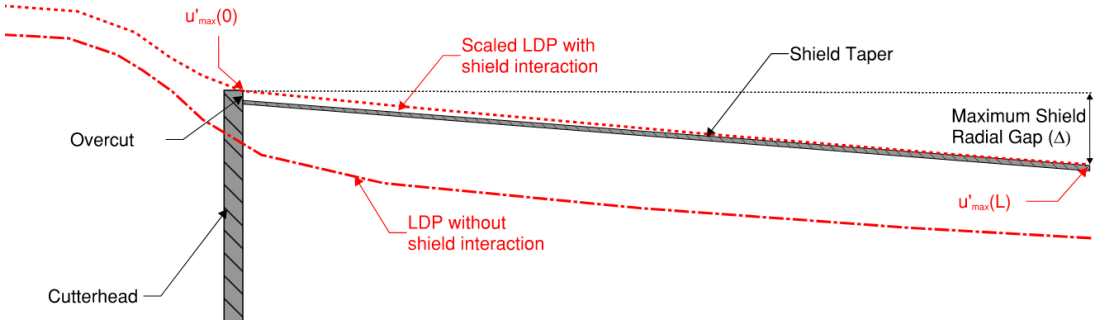

Figure 7: LDP scaling for shield gap

the well-known parametric equations by [19] which are functions of the normalized plastic radius ($R^* = \frac{r_p}{r_0}$) and final displacement at full deconfinement (u_{max}). These equations can be rearranged to obtain the displacement at the face and the shield tail by considering that the difference between the displacement at the face and the tail must be equal to the shield gap (Δ_{shield}) giving:

$$\text{Scaled maximum displacement at face:} \quad u'_{max}(0) = \frac{\Delta_{shield}}{3e^{-0.15R^*} - 1} \tag{40}$$

$$\text{Scaled maximum displacement at tail:} \quad u'_{max}(L) = u'_{max}(0) + \Delta_{shield} \tag{41}$$

The function $u'_{max}(0)$ approaches infinity at a critical value of $R^*_{crit} = \frac{ln(1/3)}{-0.15} \approx 7.32$. For urban tunnels which are usually 1 to 4 diameters from surface, at this critical plastic radius the entire soil column will have reached full plasticity. The RINGS algorithm thus incorporates this limit as an index for face instability.

The scaled displacement at the tail $u'_{max}(L)$, is used in the RINGS model to limit the formation of displacements during the incremental calculation of the elastic and plastic strains. Once the limit is reached, the algorithm stops the accumulation of strains and change of stresses towards the tunnel extrados by setting $\varepsilon_{r,t}(r_i) = \varepsilon_{r,t}(r_{i-1})$, $\gamma_{e,p}(r_i) = \gamma_{e,p}(r_{i-1})$ and $\sigma_{r,t}(r_i) = \sigma_{r,t}(r_{i-1})$.

Overall as shown, the shield interaction is indeed treated heuristically, via displacement

profile scaling. This approach is intentional because the shield-soil contact problem is highly nonlinear, dependent on lubrication, overcut, steering, and other factors, for which mechanistic derivations are not available and not usually included in design calculations including numerical modelling.

Our formulation enforces realistic displacement bounds consistent with measured shield gap effects. We view this as a practical engineering compromise that improves predictive capacity while avoiding arbitrary calibration factors.

3. PCTL Structural Model

Once the ground loading and stiffness are calculated as a function of the TBM confinement using RINGS, the PCTL ring response can be calculated.

As described by [17], the effective soil stress on the lining can be obtained utilizing the effective stress deconfinement ratio as follows:

$$\sigma'_{lining}(\theta) = (1 - \lambda) \cdot \sigma(\theta)' + \lambda \cdot P'_{SHIELD}(\theta) \tag{42}$$

Where ($\lambda = 1 - \frac{\sigma'(\theta)}{\sigma'_0(\theta)}$) is the ratio of the relaxed stress over the initial stress at each location around the tunnel perimeter following the completion of the RINGS algorithm.

The average total vertical and horizontal stresses can then be defined as: $\overline{\sigma}_v = \frac{\sigma'_v(0°)+\sigma'_v(180°)}{2} + \overline{u_w}$, $\sigma_h = K_{TBM} \cdot \sigma'_v(90° \text{ or } 270°) + \overline{u_w}$, where $\overline{u_w}$ is the average water pressure. The ground bedding stiffness is simply the average unload-reload modulus around the tunnel perimeter $E = \overline{E_{ur}}(\theta, \sigma_r)$, which has reduced compared to initial conditions due to the deconfinement process.

The lining total normal soil stress and bedding stiffness can be used as an input to any classic analytical continuum solution, like for example Duddeck-Erdmann [36] providing a reasonable estimate of lining demands and deformations as per the set of analytical equations in Table 5.

Description	Equation
Maximum Moment	Full Bond: $M_{max} = (\overline{\sigma}_v - \overline{\sigma}_h) \cdot \frac{R^2}{4 + \frac{3-2\nu}{3(1+\nu)(3-4\nu)} \cdot \frac{E_c R^3}{EJ}}$ (43) Tangential Slip: $M_{max} = (\overline{\sigma}_v - \overline{\sigma}_h) \cdot \frac{R^2}{\frac{(10-12\nu)}{(3-4\nu)} + \frac{2}{3(1+\nu)(3-4\nu)} \cdot \frac{E_c R^3}{EJ}}$ (44)
Average Hoop Thrust	$N_o = \frac{(\overline{\sigma}_v + \overline{\sigma}_h)}{2} \cdot \frac{R}{1 + \frac{1}{1+\nu} \cdot \frac{E_c R}{EA}}$ (45)
Maximum and Minimum Thrust	$N_{max,min} = N_o \pm \frac{M_{max}}{R}$ (46)
Lining Constant Deformation	$u_o = \frac{(\overline{\sigma}_v + \overline{\sigma}_h)}{2} \cdot \frac{\frac{R^2}{EA}}{1 + \frac{1}{1+\nu} \cdot \frac{E_c R}{EA} \cdot \frac{J}{AR^2}}$ (47)
Lining Maximum Deformation (Ovalization)	$u_{max} = \frac{M_{max}}{3} \cdot \frac{R^2}{EJ}$ (48)
Average Lining Convergence	$\overline{u} = u_o + \frac{u_{max}}{2}$ (49)

Table 5: Equations for Lining Forces and Deformations

It is noted that the response of the soil-lining system is assumed to be elastic post application of the ground loading. This is considered satisfactory for soft ground tunnels where the stiffness of the lining is relatively high compared to the surrounding ground [36].

It is also noted that obtaining the loads and stiffness from the RINGS model allows to use this model for both shallow and deep tunnels as it captures depth dependent stress and stiffness anisotropy.

4. Ground Loss and Surface Movements

The significant value added by ADCM is that volume or ground loss is not assumed, but derived from ground convergence (RINGS) and lining response, rather than being imposed from empirical ranges, often subject to much circular debate.

As mentioned, the tangential ground strain (ϵ_θ) is obtained from RINGS at the angular positions θ along the tunnel perimeter (radius r_0) and the average strain is computed as:

$$\overline{\epsilon}_\theta = (\frac{1}{n}) \cdot \sum_{1}^{n} \epsilon_\theta(\theta_i) \tag{50}$$

Where n is the number of discretized angular positions around the tunnel and $\epsilon_\theta(\theta_i)$ is is the tangential strain at angle θ_i.

The volume loss is then simply a sum of the average tangential strain from the RINGS model and the average net lining convergence from the PCTL structural model:

$$V_L = 100\% \cdot (\overline{\epsilon}_\theta + \left[\frac{\overline{u}}{R}\right]_{PCTL}) \tag{51}$$

Note that the backfill grout contraction while setting, is already included in the SHIELD model as part of the calculation of ΔP.

The volume loss calculated in equation [51], can be used to obtain subsurface or near-surface deformations utilizing the famous semi-empirical solution by O'Reilly and New [7] which has been shown to give similar ground surface settlements compared to analytical solutions such as [9]. The vertical surface settlement S_x at distance x from the tunnel centreline is given by:

$$S_x = -\frac{V_L \cdot \pi \cdot D_{exc}^2}{10 \cdot K_i \cdot z} \cdot e^{-\frac{x^2}{2(K_i \cdot z)^2}} \tag{52}$$

Where V_L is the volume loss as a percentage of the excavated tunnel volume, D_{exc} is

the tunnel excavated diameter. K_i is the empirical trough width parameter representing the distance from the tunnel centerline to the inflection point of the settlement trough, z is the depth from the ground surface to the tunnel axis. Experience with the ADCM supported by [6] has shown a good correlation between K_i and the Rankine active earth pressure coefficient K_a assuming the critical state friction angle ϕ_c giving a range of 0.3 to 0.5 for most soils.

4.1. Displacement-Confinement Curve

The ADCM can be used to generate a Displacement-Confinement Curve (DCC) showing the maximum surface settlement as a function of the TBM deconfinement $(1 - \lambda_{TBM}(\theta))$ for a given set of ground and TBM parameters. An example of the DCC at $\theta = 90°$ (i.e. springline) is illustrated in Figure 8 for an 8m diameter tunnel at a depth of 33m with a water depth of 27m in sandy silts with a friction angle of 32 degrees, $E_{ur} = 45$ MPa, $r_u = 1.5$ and $K_{TBM} = 0.4$ for a range of shield gap values. Grouting pressure is assumed at 0.5bar above the earth pressure at the tunnel crown.

As discussed in Section 2.2.3, an optimal range of λ_{TBM} between 0.2 and 0.8 corresponds to a surface settlement response that indicates soil stability and control over ground movements. At the under-pressurized range, the DCC shows increased ground movements eventually leading to loss of face stability when the plastic radius exceeds the tunnel depth. At the over-pressurized zone, it is shown that for all shield gap values, an increase in face pressure has negligible impact on the surface movements and working at this level will be detrimental to the TBM productivity with unnecessarily high thrust forces and tool wear. In addition, the interaction with the shield is clearly demonstrated for the lower shield gap of 25mm which limits the amount of volume loss up to failure but results in high frictional resistance along the advancing shield.

The DCC can thus be used to set surface settlement triggers that are directly related to the TBM operation and design. This is a powerful tool for real-time TBM operation and risk management.

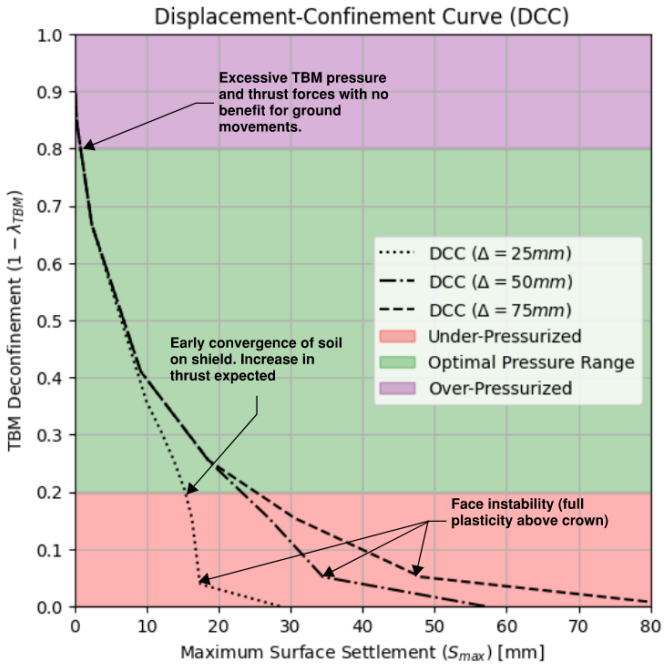

Figure 8: DCC example for a for a deep tunnel with cover to diameter ratio of $(H - D_{exc})/D_{exc} = 3$, demonstrating behavior for a range of shield gap values

5. Validation and Case Studies

The ADCM is validated on five case histories of completed TBM tunnels in soft ground which are listed in Table 6, and for which the source for the data is provided in the references. These include both shallow and deep tunnels constructed using EPBMs and Slurry TBMs of different diameters driven in various ground conditions around the world. The key inputs for each study are summarized in Tables 6 to 8 with the TBM parameters illustrated in Figure 1 above. The large variability reinforces the robustness of ADCM.

For cases 1 and 2, the MCSH soil parameters were taken directly from the available literature. For the rest of the cases, the parameters were derived from either MC or CamClay model parameters which were given by the authors using standard relationships. This proves the simplicity of the ADCM data requirements.

For all case studies the PCTL properties were $f_c = 50$ MPa, $E_c = 35$ MPa, $\nu = 0.2$. For all cases except 4, it was assumed that the lining is Fiber Reinforced Polymer (FRP) with concrete capacity per RILEM [37] recommendations. For Case Study 4, the lining was conventional reinforced concrete with 0.5% reinforcement ratio per the information

in [38]. The parameter m_g was set as 0 for EPBMs and 1 for Slurry TBMs.

The ADCM calculations for each case study are provided in Figures 9 to 14.

No.	Case Study	Monitoring Section(s)	Year	Location	Source	Ground Conditions at Face	TBM Type
1(a,b)	Tunnelling and Limitation Impact on Piles (TULIP)	(a)SMRN; (b)SMRS	2023	Paris, France	[39], [40]	Fine clayey sands with sandstone inclusions	EPBM
2	Barcelona Line 9	Chainage,PK 4+150	2018	Barcelona, Spain	[41]	Deltaic silty clays interbedded with sands, sandy silts, silts and clays	EPBM
3	Tianjin Metro Line 5	Test Section C	2018	Tianjin, China	[42]	Soft clays and silts	EPBM
4	Lyon Subway Line D Extension	Test Section S1	1997	Lyon, France	[43]	Clay with a sand layer	Slurry
5	Tsinghua-Yuan Tunnel	Chainage 17+885	2020	Beijing, China	[44]	Silty clay with pebble sand	Slurry

Table 6: Summary of tunnel case studies

Case Study	H (m)	H_w (m)	D_{exc} (m)	L (m)	Δ (mm)	D_{ext} (m)	D_{int} (m)	P_{face} (bar)	P_{grout} (bar)	$\overline{P}_{SHIELD}$ (bar)
1a	21.0	9.5	9.87	11	35	9.5	8.7	1.8	2.4	2.3
1b	21.0	9.5	9.87	11	35	9.5	8.7	1.8	2.2	2.0
2	20.2	19.2	9.43	11.4	80	8.75	8.11	2.6	3.1	2.8
3	26.0	26.0	6.4	8.7	25	6.2	5.5	2.5	3.7	3.7
4	16.9	8.6	6.27	7.0	15	6.0	5.3	1.1	1.6	1.6
5	23.0	-	12.6	14.0	220	11.95	10.85	1.3	4.5	4.5

Table 7: Case histories tunnel geometry and recorded TBM pressures at springline

Case Study	γ (kN/m^3)	γ_b (kN/m^3)	φ (°)	c' (kPa)	E_{ur}^{ref} (MPa)	E_{50}^{ref} (MPa)	ν	K_{tbm}	m	P'_{ref} (kPa)
1	20	14	33	10	60	20	0.2	0.45	0.5	100
2	20	14	30	10	39	13	0.2	0.5	0.8	100
3	20	14	27	0	13.5	3.5	0.2	0.4	1.0	100
4	20	12	31	15	39	13	0.2	0.35	1.0	100
5	20	12	18	34	45	15	0.2	0.5	1.0	100

Table 8: Soil and TBM fluid properties at tunnel face

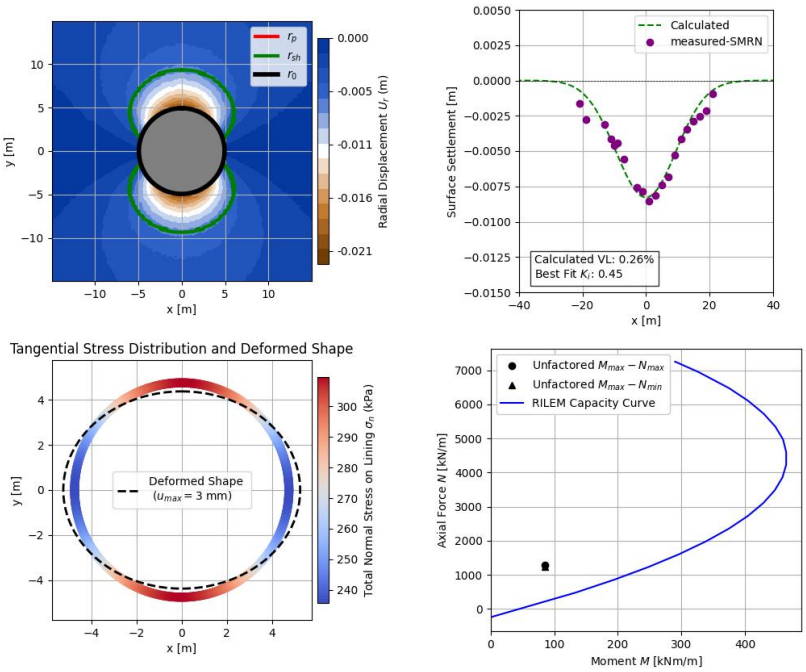

Figure 9: Back-analysis results - Case Study 1a (SMRN); $\lambda_{TBM}(\theta = 0°) = 0.64$.

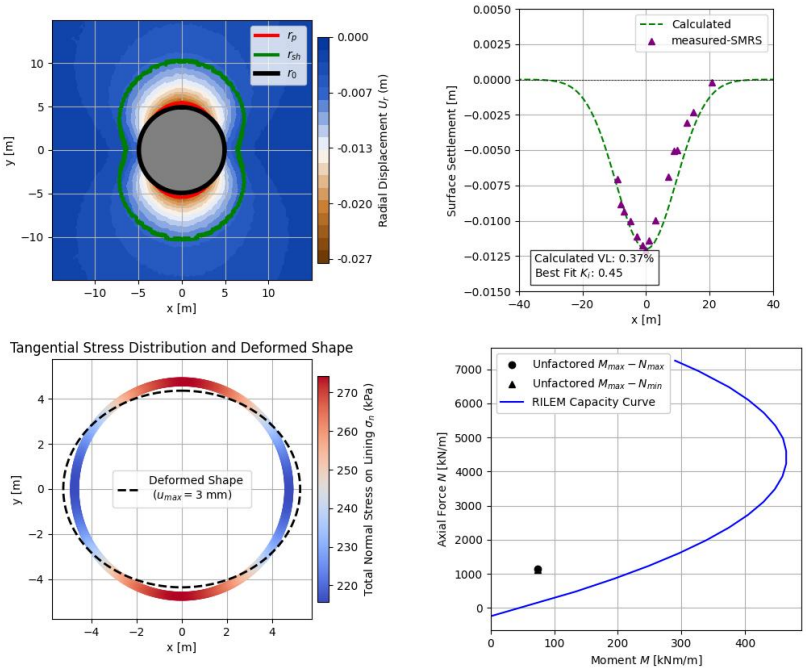

Figure 10: Back-analysis results - Case Study 1b (SMRS); $\lambda_{TBM}(\theta = 0°) = 0.73$.

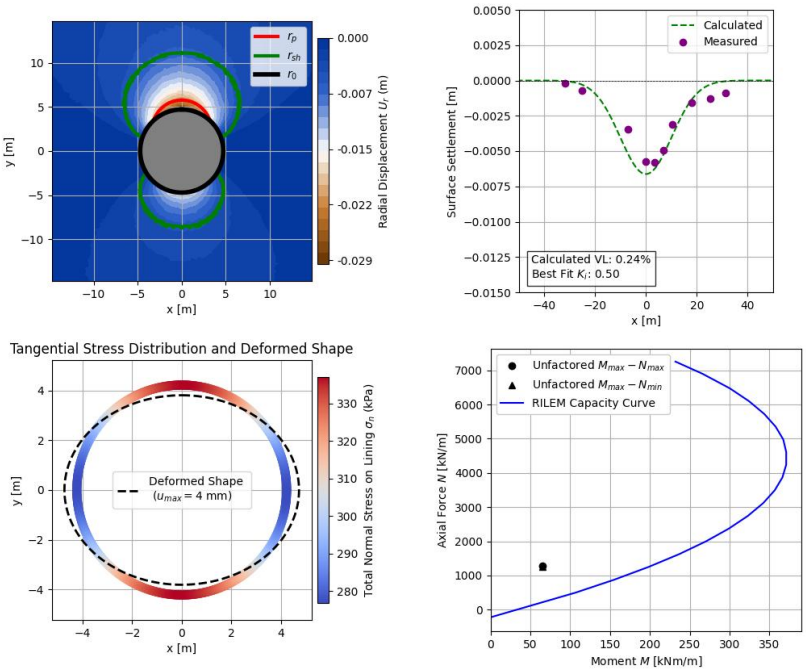

Figure 11: Back-analysis results - Case Study 2; $\lambda_{TBM}(\theta = 0°) = 0.67$.

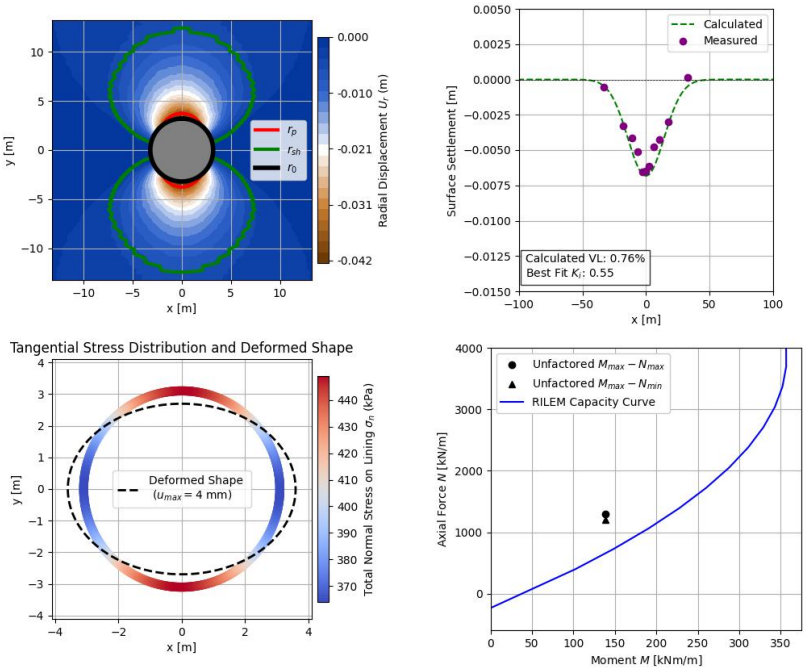

Figure 12: Back-analysis results - Case Study 3; $\lambda_{TBM}(\theta = 0°) = 0.57$.

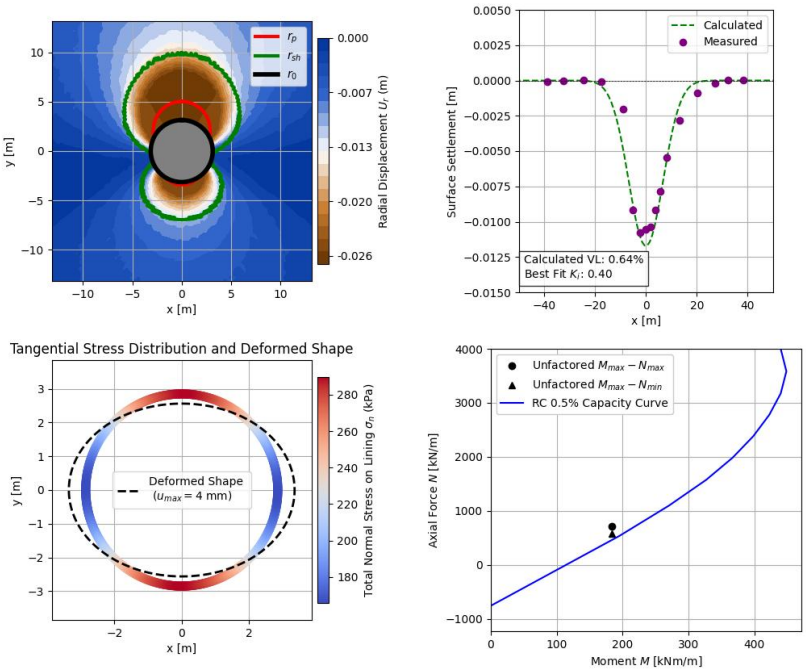

Figure 13: Back-analysis results - Case Study 4; $\lambda_{TBM}(\theta = 0°) = 0.92$.

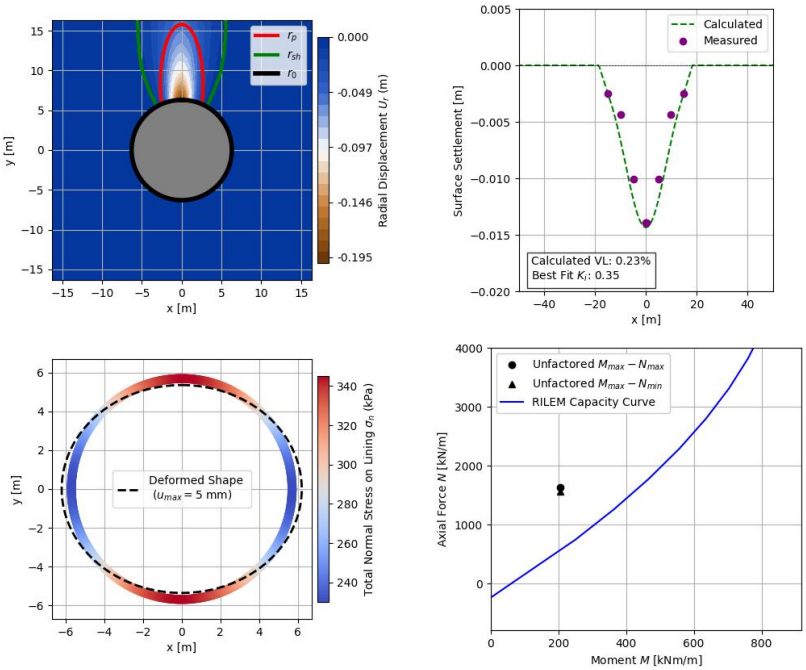

Figure 14: Back-analysis results - Case Study 5; $\lambda_{TBM}(\theta = 0°) = 0.85$.

5.1. Discussion

5.1.1. Ground movements and soil behaviour

The back-analysis results show a very good match between the ADCM and the measured settlement troughs with an average error of less than 5% compared to all surface monitoring points.

As already mentioned, a key ADCM advantage is the ability to calculate the volume loss directly as a function of the TBM and ground parameters, all of which can be explicitly measured. As shown, calculated volume losses fit well within the typical range of closed-face TBM tunnels in soft ground normally between 0.5% and 1% [45], with larger diameter tunnels giving lower values corresponding to the observations discussed by [2].

The standard input material parameters K_0 and OCR in numerical modelling, are replaced in the ADCM with the mobilized TBM horizontal stress ratio K_{tbm}. The back analyzed values for this parameter are all within a narrow range of 0.35 to 0.5, with lower values approaching K_a for smaller diameter tunnels and higher values approaching K_0 for the larger diameter tunnels. This is an interesting correlation as the horizontal stress ratio in soils is a function of the mobilized strain. Therefore, for larger diameter tunnels, where their average strain (i.e. volume loss) is generally lower, the stress ratio approaches the in-situ value and vice versa for smaller diameter tunnels.

The calculated TBM confinement ratio λ_{TBM} at the tunnel crown, is in most cases within the range of 0.6 to 0.8 which is considered optimal. Case 4 is the exception where the value of 0.92 indicates an under-pressurized state and where the soil is shown to converge on the TBM shield reaching the u_{max} cap. The reason that the movements are generally well controlled in this case at $S_{max} = 11.5$mm, is according to the ADCM analysis purely due to $\Delta = 15$mm.

Case 5, with a slightly under-pressurized value λ_{TBM} of 0.85, a significant difference between the slurry and grouting pressure (3 bar) and a large $\Delta = 220$mm, results in large

deformations of almost 200mm localized at the tunnel crown. However, due to the size and depth of the tunnel, the surface settlements are still within acceptable limits, albeit with a particularly narrow trough width. This is consistent with the monitoring results for horizontal movements presented in [44] around the tunnel axis which are limited to 1-2mm. The latter was explained by the authors of this cases study as a result of cross-anisotropic soil stiffness. However the ADCM captures this behaviour as a function of the geometry and confinement provided by the TBM.

The fitted values for K_i are all within the typical range of 0.3 to 0.5 for soft ground tunnels [7]. However, this parameter has no impact on the calculations and is required here only due to the chosen transfer function. Other analytical or empirical methods such as [9] or [6] or a 2D numerical model with an imposed volumetric strain or prescribed convergence can be used equally well relieving the requirement to calibrate this parameter.

It is worth noting that the match for the ground loss and surface settlement trough captured for the TULIP benchmark (Case 1), matches exactly with the reported values in [40] and is significantly better than most, if not all, of the 17 independent 2D and 3D numerical studies presented in [39] for both monitored sections. The ADCM points to the increased settlement in section SMRS compared to SMRN purely due to the lower recorded grouting pressure. This match is not artificial - it is the most simple explanation of the difference in settlements between the two sections which are otherwise largely identical.

Finally, it is noted that the match to final measured settlements was achieved without accounting for excess pore pressure effects in the MCSH or considering soil stratigraphy, as volume loss is primarily governed by face conditions controlling ground behaviour in greenfield scenarios. Excess pore pressure effects are mitigated by designing earth pressures to exceed pore pressures, with consolidation dissipating rapidly even in low-permeability soils and moderate oedometer stiffness. Observations from the case studies analyzed show minimal ground movement changes post-TBM passage, attributed mostly to backfill grout setting. Significant long-term settlements around tunnels on other projects are more likely due to external factors, such as nearby excavations, tunnel waterproofing

issues, or groundwater table lowering.

5.1.2. Lining behaviour and utilization

The ADCM also allows capturing lining loading and stiffness from the RINGS model and then linking the lining demands to the volume loss and TBM pressures. The lining maximum demands from all case histories sit within the capacity curve, validating observations of no excessive cracking and reported lining instabilities.

As expected, higher moment utilization is observed in cases 3 and 4 corresponding to higher volume loss. For the larger diameter tunnels in cases 1, 2 and 5, moment utilization is lower due to the reduced ground loss.

The latter observation is particularly important due to the increased interest in the construction of large diameter tunnels and the recent trends to use fibre-reinforced concrete wherever possible. While, it is intuitive to associate a large diameter tunnel with higher lining demands, the ADCM shows that this is not necessarily the case in practice as the lining demands are a function of the volume loss which is generally lower and is assisted by the high TBM face and grouting pressures required to maintain face stability and maintain a reasonable advance rate.

6. Summary and Conclusions

This paper presents the Advanced Displacement-Confinement Method (ADCM), a novel semi-analytical framework designed to evaluate ground-structure interaction in closed-face mechanized shield tunnelling under soft ground conditions and in the short-term due to the avoidance of pore water pressure considerations.

Integrating several independent analysis algorithms, the ADCM allows direct estimation of TBM pressure distributions, ground deformations, and lining demands.

Its constitutive modelling incorporates elasto-plastic shear hardening behaviour, address-

ing anisotropy, shield interaction, and lining flexibility with analytical clarity.

Validation through multiple case studies demonstrates that ADCM effectively predicts settlement troughs and lining demands consistent with field measurements.

The method exhibits significant computational efficiency and transparency, particularly valuable in early design and parametric studies.

In addition, due to the simplicity and efficiency of the ADCM targeting measurable known quantities on any soft ground TBM project, it is envisaged as an invaluable tool for back-analysis and in particular, real-time monitoring and setting and interpretation of trigger levels. This is a key component that is links the design of the tunnel to the impact on the existing conditions which is often the most difficult aspect of tunnelling in a dense urban environment.

Future work will focus on developing and demonstrating the advantages of using ADCM for back-analysis in conjunction with monitoring and TBM data in real-time and incorporation of mitigation measures such as injection of thixotropic agents around the shield.

Acknowledgements

The authors would like to acknowledge the technical discussions with Kiewit and JV partners that led to the development of the ADCM. We would also like to thank the TULIP project team for providing the raw monitoring data for Case Study 1. Special thanks to Dr Benny Guralnik and Mr Michan Condra ing. for their insights and contributions.

Declaration of generative AI and AI-assisted technologies in the manuscript preparation process: During the preparation of this work the author(s) used GitHub Copilot and OpenAI ChatGPT in order to assist with code generation and text suggestions. After using this tool/service, the author(s) reviewed and edited the content as needed and take(s) full responsibility for the content of the published article.

References

[1] B. Maidl, M. Herrenknecht, U. Maidl, G. Wehrmeyer, Mechanised Shield Tunnelling, Wiley, 2012. doi:10.1002/9783433601051.

[2] E. J. Cording, Monitoring and controlling ground behavior at the source: Recent applications to pressurized tunneling, Sir Alan Muir Wood Lecture, World Tunnel Congress (WTC 2018), Dubai, UAE, presented at the 44th ITA Annual Meeting and World Tunnel Congress, 21–25 April 2018 (2018).

[3] X. chun Zhong, Q. wei Liu, H. Zhao, Study on the Grouting Pressure of Shield Tunnel, pp. 183–190. doi:10.1061/47626(405)23.

[4] M. S. P. Wan, J. R. Standing, D. M. Potts, J. B. Burland, Measured short-term subsurface ground displacements from epbm tunnelling in london clay, Géotechnique (2017). doi:10.1680/jgeot.sip17.p.148.

[5] G. Zheng, Q. Fan, T. Zhang, Q. Zhang, Numerical study of the soil-tunnel and tunnel-tunnel interactions of epbm overlapping tunnels constructed in soft ground, Tunnelling and Underground Space Technology 124 (2022) 104490. doi:10.1016/j.tust.2022.104490.

[6] N. Loganathan, H. Poulos, A. Bustos-Ramirez, Estimation of ground loss during tunnel excavation.

[7] M. O'Reilly, B. New, Settlement above tunnels in the united kingdom — their magnitude and prediction, International Journal of Rock Mechanics and Mining Sciences Geomechanics Abstracts 20 (1) (1983) A18. doi:10.1016/0148-9062(83)91768-0.

[8] A. Verruijt, J. R. Booker, Surface settlements due to deformation of a tunnel in an elastic half plane, Géotechnique (1996). doi:10.1680/geot.1996.46.4.753.

[9] C. Sagaseta, Analysis of undrained soil deformation due to ground loss, Géotechnique 37 (3) (1987) 301–320. doi:10.1680/geot.1987.37.3.301.

[10] M. Panet, A. Guenot, Analysis of convergence behind the face of a tunnel, International Journal of Rock Mechanics and Mining Sciences & Geomechanics Abstracts 20 (1) (1983) A16. doi:10.1016/0148-9062(83)91744-8.

[11] C. Carranza-Torres, B. Rysdahl, M. Kasim, On the elastic analysis of a circular lined tunnel considering the delayed installation of the support, International Journal of Rock Mechanics and Mining Sciences 61 (2013) 57–85. doi:10.1016/j.ijrmms.2013.01.010.

[12] A. Vrakas, Analysis of ground response and ground-support interaction in tunnelling considering large deformations, Doctoral thesis, ETH Zurich, Zurich (2016). doi:10.3929/ethz-a-010778160.

[13] A. Vrakas, W. Dong, G. Anagnostou, Elastic deformation modulus for estimating convergence when tunnelling through squeezing ground, Géotechnique (2018). doi:10.1680/jgeot.17.p.008.

[14] M. Anthi, T. Pferdekämper, G. Anagnostou, Analytical solutions for cavity contraction in strain-softening materials with linear or exponential strength decay, Scientific Reports (2024). doi:10.1038/s41598-024-65186-y.

[15] Y.-L. Lee, Explicit procedure and analytical solution for the ground reaction due to advance excavation of a circular tunnel in an anisotropic stress field, Geotechnical and Geological Engineering (2018). doi:10.1007/s10706-018-0537-4.

[16] C. Guo, K. Han, H. Kong, L. Shi, Explicit form of exact analytical solution for calculating ground displacement and stress induced by shallow tunneling and its application, Advances in Civil Engineering 2019 (1) (2019) 5739123. doi:10.1155/2019/5739123.

[17] E. Almog, M. Mangione, G. Cachia, Ground relaxation in segmental lining design using the convergence-confinement method, in: Underground Design and Construction Conference, IOM3 Hong Kong Branch, 2015, pp. 335–345.

[18] P. Aristaghes, P. Autuori, Calcul des tunnels au tunnelier, Revue Française de Géotechnique (97) (2001) 31–40. doi:10.1051/geotech/2001097031.

[19] N. Vlachopoulos, M. S. Diederichs, Improved longitudinal displacement profiles for convergence confinement analysis of deep tunnels, Rock Mechanics and Rock Engineering 42 (2) (2009) 131–146. doi:10.1007/s00603-009-0176-4.

[20] E. Brown, J. Bray, B. Ladanyi, E. Hoek, Ground response curves for rock tunnels, International Journal of Rock Mechanics and Mining Sciences & Geomechanics Abstracts 20 (4) (1983) 112–113. doi:10.1016/0148-9062(83)91081-1.

[21] T. Kasper, G. Meschke, A 3d finite element simulation model for tbm tunnelling in soft ground, International Journal for Numerical and Analytical Methods in Geomechanics 28 (2004) 1441 – 1460. doi:10.1002/nag.395.

[22] M. A. Mooney, J. Grasmick, B. Kenneally, Y. Fang, The role of slurry tbm parameters on ground deformation: Field results and computational modelling, Tunnelling and Underground Space Technology (2016). doi:10.1016/j.tust.2016.01.007.

[23] ITA Working Group 2, Guidelines for the Design of Segmental Tunnel Linings, International Tunnelling Association (ITA), 2019.

[24] E. Bourgeois, N. Berthoz, W. Mohamad, F. Szymkiewicz, A. L. Kouby, D. Branque, A. Michalski, C. Kreziak, L. Soyez, Results of a benchmark exercise of prediction of tunnel-pile interaction: The tulip project, in: Proceedings of the International Society for Soil Mechanics and Geotechnical Engineering (ISSMGE), 2023.

[25] H. Yeow, G. Katsigiannis, Application of numerical modelling in Next Generation of Eurocode 7, CRC Press, 2024, pp. 2037–2042. doi:10.1201/9781003431749-383.

[26] Z. Zizka, M. Thewes, DAUB Recommendations for Face Support Pressure Calculations for Shield Tunnelling in Soft Ground, 2016.

[27] T. Dias, A. Bezuijen, Grout pressure distribution during tbm tunnelling, 2017.

[28] D. M. Potts, L. Zdravkovic, Finite element analysis in geotechnical engineering: Application, Thomas Telford Publishing (2002) 1–427doi:10.1680/feaigea.29904.

[29] C. Gong, W. Ding, D. Xie, Twin epb tunneling-induced deformation and assessment of a historical masonry building on shanghai soft clay, Tunnelling and Underground Space Technology 99 (2020) 103300. doi:10.1016/j.tust.2020.103300.

[30] M. Cudny, A. Truty, Refinement of the hardening soil model within the small strain range, Acta Geotechnica 15 (2020) 2031–2051. doi:10.1007/s11440-020-00945-5.

[31] S. C. Möller, P. A. Vermeer, On numerical simulation of tunnel installation, Tunnelling and Underground Space Technology 23 (4) (2008) 461–475. doi:10.1016/j.tust.2007.08.004.

[32] J. P. Janin, et al., Numerical back-analysis of the southern toulon tunnel: modelling and monitoring results, Tunnelling and Underground Space Technology 47 (2015) 235–251. doi:10.1016/j.tust.2015.03.020.

[33] B. Simpson, Retaining structures: displacement and design, Géotechnique 42 (4) (1992) 541–576. doi:10.1680/geot.1992.42.4.541.

[34] T. Schanz, P. Vermeer, P. Bonnier, The hardening soil model: Formulation and verification (2019). doi:10.1201/9781315138206-27.

[35] T. A. Bower, A. D. Jefferson, P. J. Cleall, A reformulated hardening soil model, Proceedings of the Institution of Civil Engineers - Engineering and Computational Mechanics (2020). doi:10.1680/jencm.18.00054.

[36] H. Duddeck, J. Erdmann, On structural design models for tunnels in soft soil, Underground Space 9 (1985) 246–259.

[37] RILEM Technical Committee 162-TDF, Rilem tc 162-tdf: Test and design methods for steel fibre reinforced concrete: sigma-epsilon design method, final recommendation, Materials and Structures 36 (2003) 560–567.

[38] S. Bernat, Modélisation du creusement d'un tunnel en terrain meuble : qualification sur chantier expérimental, Ph.D. thesis, thèse de doctorat dirigée par Cambou, Bernard Sciences appliquées Ecully, Ecole centrale de Lyon 1996 (1996).

[39] N. Berthoz, D. Branque, A. Michalski, W. Mohamad, E. Bourgeois, A. L. Kouby, F. Szymkiewicz, A. Rallu, Impact of tunnelling on piles in parisian subsoil: dataset of in-situ measurements in the ground and on three instrumented piles, Data Brief 47 (2023) 108971. doi:10.1016/j.dib.2023.108971.

[40] A. Michalski, D. Branque, N. Berthoz, A. Rallu, W. Mohamad, F. Szymkiewicz, A. L. Kouby, E. Bourgeois, Greenfield response to epbm tunneling in paris and relations with tbm operation variables, Journal of Geotechnical and Geoenvironmental Engineering 150 (10) (2024) 05024011. doi:10.1061/JGGEFK.GTENG-12136.

[41] M. T. Yubero, E. Bonet, Ground surface effect of earth pressure balance tunnelling in deltaic deposits: A case study of line 9 of the barcelona metro, Sustainability 16 (18) (2024). doi:10.3390/su16188275.

[42] G. Zheng, Q. Fan, T. Zhang, Q. Zhang, Numerical study of the soil-tunnel and tunnel-tunnel interactions of epbm overlapping tunnels constructed in soft ground, Tunnelling and Underground Space Technology 124 (2022) 104490. doi:10.1016/j.tust.2022.104490.

[43] M. Beghoul, R. Demagh, Slurry shield tunneling in soft ground. comparison between field data and 3d numerical simulation, Studia Geotechnica et Mechanica 41 (3) (2019) 115–128. doi:10.2478/sgem-2019-0003.

[44] J. Cui, W.-H. Xu, Y. Fang, L.-M. Tao, C. He, Performance of slurry shield tunnelling in mixed strata based on field measurement and numerical simulation, Advances in Civil Engineering 2020 (2020). doi:10.1155/2020/6785260.

[45] B. New, E. Leca, Settlements induced by tunneling in soft ground, Tunnelling and Underground Space Technology 22 (2) (2007) 119–149. doi:10.1016/j.tust.2006.11.001.